Nuclear Instruments and Methods in Physics Research A277 (1989) 418–430
North-Holland, Amsterdam

HEAVY ION SEPARATION WITH A GAS-FILLED MAGNETIC SPECTROGRAPH

Michael PAUL *, Bruce G. GLAGOLA, Walter HENNING **, Jörg G. KELLER **, Walter KUTSCHERA, Zenhao LIU +, Karl Ernst REHM, Bernhard SCHNECK ++ and Rolf H. SIEMSSEN §

Physics Division, Argonne National Laboratory, Argonne, IL 60439, USA §§

Received 27 December 1988

Heavy ions passing through a magnetic field region filled with gas experience atomic charge-changing collisions and follow trajectories approximately determined by the mean charge state in the gas. The properties of a gas-filled Enge magnetic spectrograph are studied in detail by measuring focal-plane position spectra of fast heavy ions and their evolution as a function of gas pressure. The method allows physical separation of pairs of isobaric ions in the focal plane. Applications in accelerator mass spectrometry experiments are described. At intermediate low pressures, single atomic charge-changing processes can be identified. A Monte Carlo simulation program of the ion transport through the gas-filled magnet is developed and reproduces closely the experimental behavior.

1. Introduction

Magnetic spectrographs have been widely utilized for the detection and identification of light and heavy ions. The magnetic rigidity, given by the momentum of the ion divided by its electric charge, governs the trajectory of the ion in a magnetic field region and is normally a constant throughout the path of the ion in vacuum. The dispersion for ions with different magnetic rigidities results in a spatial distribution in the focal plane of the apparatus, which can be measured often with high resolution. Together with other parameters like energy or velocity, it can be used for the identification of the ion. The situation is complicated for heavy ions by the fact that, after passage through matter (e.g. target, absorber, foil window), the ions emerge with a distribution of ionic charge states; these ions follow different trajectories in the magnetic field, as determined by their charge state. On the other hand, for ions with the same mass numbers (isobaric nuclei), which are the main topic of the present work, the trajectories will be essentially identical if the ions have the same energy and the same charge state; such ions are therefore not separated by the spectrograph.

If, however, the magnetic field region is filled with gas, the ions will undergo atomic collisions in which electrons can be lost or captured, changing the charge states of the ions. The situation is schematically illustrated in fig. 1 for heavy ions moving in vacuum and in a gas-filled magnetic region. If the mean free path of the ions between the charge-changing collisions is short enough, depending on the gas pressure and the atomic collision cross sections, the ions will closely follow the trajectory determined by the mean magnetic rigidity, corresponding to the mean charge state of the ion. This technique has been originally proposed by Cohen and Fulmer [1] and later by Armbruster et al. [2,3] for the separation of the nuclei within an isobaric chain of fission products. Indeed, for such ions with the same mass numbers but with different atomic numbers, the mean charge state in the gas is different and the corresponding trajectories in the magnetic field are therefore spatially separated. Moreover, because the average charge $\bar{q}$ of the ion depends on the atomic number Z and is roughly proportional to its velocity, the average magnetic rigidity ($\langle B\rho \rangle \propto mv/\bar{q}$) is almost independent of the velocity distribution of the ions. The corresponding trajectories will therefore be mainly determined by the mass number A and the atomic number Z of the ion, resulting in a nearly velocity independent focus for the ions. Two competing processes will determine the degree of separation of these trajectories, namely the statistics of the charge-changing collisions and the

* Permanent address: Racah Institute of Physics, Hebrew University, Jerusalem 91904, Israel.
** Permanent address: GSI Darmstadt, D-6100 Darmstadt, FRG.
+ On leave from Institute of Modern Physics, Lanzhou, People's Republic of China.
++ On leave from Physics Department, Technical University of Munich, D-8046 Garching, FRG.
§ Permanent address: Rijksuniversiteit, Groningen, The Netherlands.
§§ Work supported by the US Department of Energy, Nuclear Physics Division, under Contract W-31-109-ENG-38.

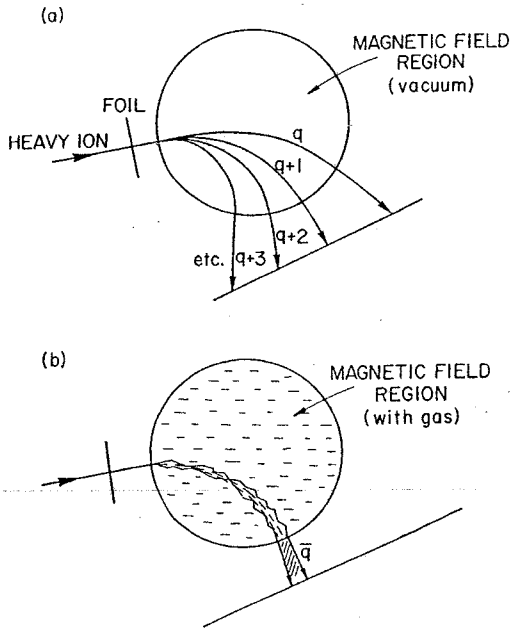

Fig. 1. Schematic illustration of the trajectories followed by heavy ions in a magnetic field region: (a) in vacuum; (b) in a gas. In the gas-filled magnetic field region, the discrete trajectories corresponding to the different charge states coalesce around a trajectory defined by the mean charge state of the ion in the gas.

broadening due to the angular and energy loss straggling. Some more recent applications of gas-filled magnetic separation are given in refs. [4–6].

In the present work, we mainly seek to study the method of gas-filled magnetic separation for the detection of rare isotopes in accelerator mass spectrometry (AMS) measurements (for recent reviews of the AMS technique see refs. [7,8] and references therein). The detection of nuclei at very low abundances (e.g. long-lived radioactive nuclei produced in nature by interaction of cosmic rays with matter) is usually hampered by the background originating from stable isobaric nuclei present in matter at concentrations higher by many orders of magnitude. It is shown that the use of a gas-filled magnet results in a much improved isobar separation, allowing measurements which were previously impractical. The measurements reported here were made with a broad-range Enge split-pole magnetic spectrograph equipped with a focal-plane heavy-ion detector; the apparatus is described in section 2. Section 3 presents a systematic experimental study of the behavior of the charge-state spectrum as a function of gas pressure for different ions (^{41}K, ^{58}Ni and ^{126}Te). Experimental data on isobaric separation with the gas-filled split-pole spectrograph are presented in section 4, together with some applications on AMS measurements. A microscopic description of the process and a Monte Carlo simulation model are described in section 5. The special case of passage of ions through gas at intermediate low pressures (10^{-3} to 10^{-2} Torr) is examined in section 6. The results are summarized in section 7.

2. The Enge split-pole magnetic spectrograph

The split-pole magnetic spectrograph, used in the present experiments, has been described by Enge et al. [9,10] and is illustrated in fig. 2. Its main components are two magnetic dipoles enclosed in a single coil and separated by a region with lower magnetic field. The purpose of the split between the pole pieces is to provide second-order double-focusing over a broad range of momenta. As described in detail in ref. [9], this is achieved by a combination of particular pole piece boundary shapes and their location and angles with respect to each other and to the focal plane. The length of the ion trajectory from the entrance slits to the focal-plane varies from 230 to 280 cm between both ends of the detector. Actual dimensions and parameters of the pole pieces are defined and listed in section 4. In the present experiments, the whole magnet chamber, i.e. the region between the entrance slits to the spectrograph and the focal-plane detector, was filled with nitrogen gas which was kept at constant pressure. A 1.5 μm thick Mylar foil (see fig. 2 for details) was mounted 7.5 cm in front of the entrance slits of the spectrograph to separate the gas in the magnet from the high vacuum (10^{-6} Torr) in the target chamber.

The focal-plane detector has been described by Erskine et al. [11]. The active part of the detector, positioned along the focal surface, covers a momentum range of $p_{max}/p_{min} = 1.3$. The detector is a combination of a gridded ionization chamber and position-sensitive proportional counters. For the ions detected here, it was operated with freon gas (CF_4) around a pressure of 100 Torr; the entrance window of the detector is a 2.5 μm thick clear Mylar foil. The position along the focal plane for an ion entering the detector is measured independently by two parallel resistive wires which are the anodes of the proportional counters. Differential energy loss signals are available from the split anode of the ionization chamber. A total energy signal (energy of the ion after the detector entrance foil) is extracted from the cathode of the detector, capacitively coupled to the grid. Details on the construction and the properties of the detector can be found in ref. [11] and regarding its particular application to AMS measurements, in ref. [12].

3. Evolution of focal plane position spectra with pressure: experimental results

The broad-range character of the split-pole magnetic spectrograph permits a detailed study of the transport

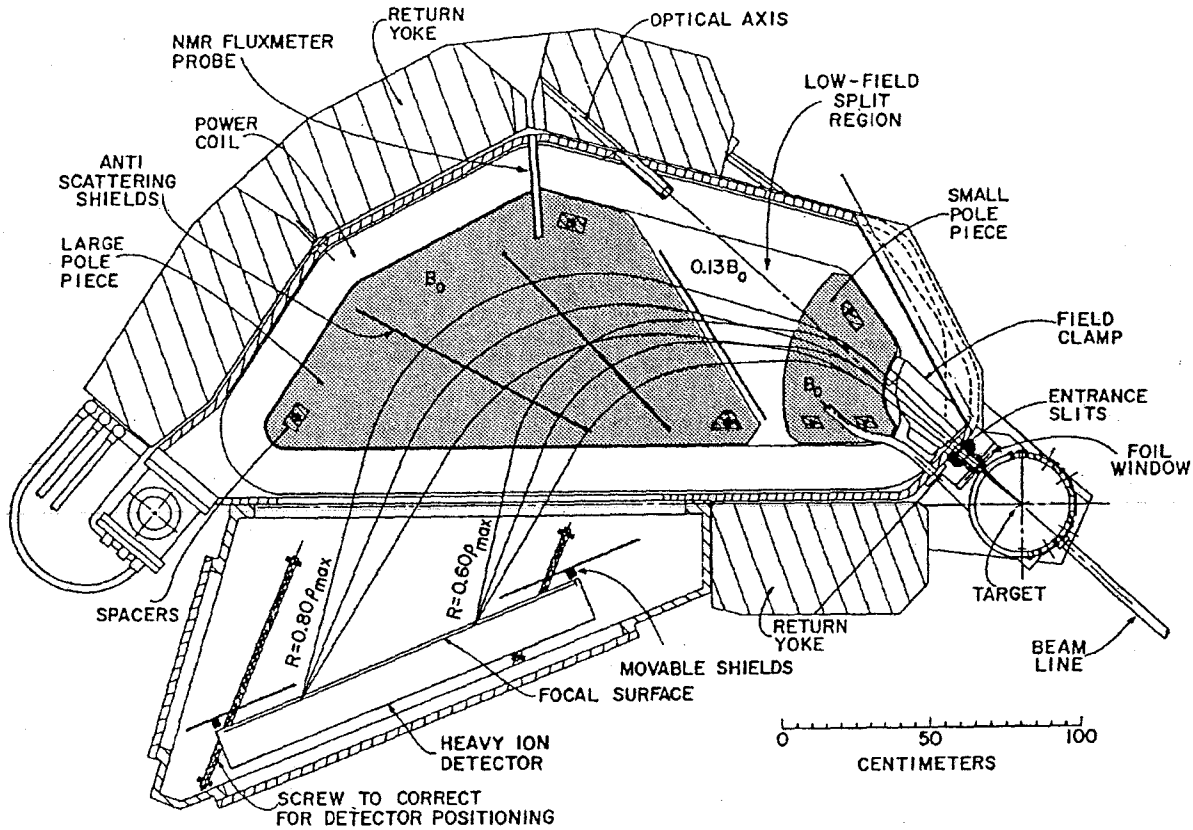

Fig. 2. Top view of the Enge split-pole spectrograph [9,10]. The spectrograph is shown here equipped with the focal-plane heavy-ion detector [11] used in the present measurements. Trajectories corresponding to low and high magnetic rigidities accepted in the detectors are shown. The whole chamber of the magnet was filled with nitrogen gas. The gas pressure was monitored by a capacitive pressure gauge and kept constant to within 0.01 Torr. The foil window (1.5 μm thick clear Mylar), used to contain the gas, is shown. The window was placed between the entrance scattering chamber and a valve (not shown in the figure); the window could thus be exchanged by closing the valve without pumping out the spectrograph chamber. The dimensions of the rectangular entrance slit to the spectrograph are 3.6 cm and 1.1 cm in the horizontal and vertical directions respectively.

of ions through the gas. In this section, we present results of such a study. Fast heavy ions were obtained from the ATLAS accelerator facility at Argonne National Laboratory and were scattered off a 200 $\mu g/cm^2$ thick Au target at an angle of 20°, placed at the object position (target) of the spectrograph (see fig. 2).

Figs. 3a–k illustrate the dependence of the focal-plane position spectra on gas pressure in the spectrograph for ^{58}Ni ions with 350 MeV incident energy and an incident charge state of 18+. The magnetic field of the spectrograph was adjusted to keep the charge-state distribution approximately centered on the focal-plane detector. The spectrum measured with high vacuum conditions in the magnet chamber ($P_{N_2} = 10^{-6}$ Torr) shows the discrete peaks obtained from the charge state distribution of the ions after their passage through the entrance foil to the magnet chamber. It is important to notice in fig. 3 that with the increase in gas pressure from the high-vacuum regime to pressures of the order of 1 Torr, the charge state distribution changes gradually from the distribution of the ions in the solid foil material to the distribution in the gas medium. The latter is known to be characterized by a mean charge state smaller than in solid, resulting therefore in stiffer particles. The corresponding shift in the centroid of the spectrum can be observed in a comparison between figs. 3a and 3d. (Note the change in magnetic field strength from 1.270 T to 1.426 T).

At higher pressures a different phenomenon occurs. Although the mean charge state decreases when the ions slow down, the magnetic rigidity decreases progressively along the ion path because the ions lose energy passing through the gas. This can be observed in the spectra of figs. 3f–k. The particular case of intermediate low pressures (in the range of 10^{-3} to 10^{-2} Torr) and the appearance of satellite peaks near the main charge states (see figs. 3b and c) is discussed in detail in section 6.

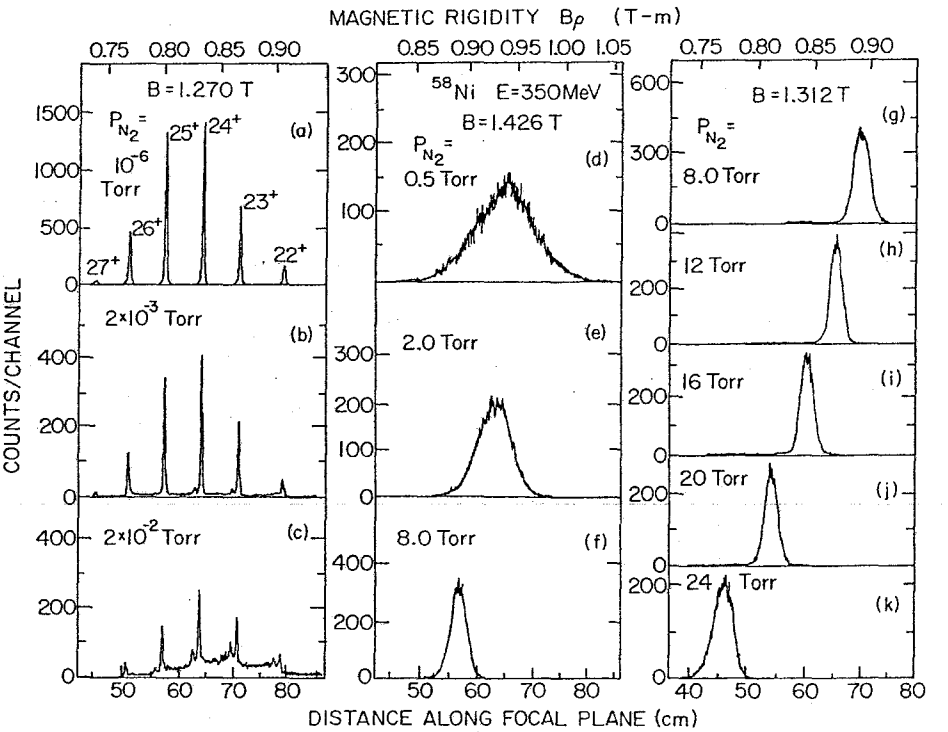

Fig. 3. Focal-plane position spectra for ^{58}Ni ions with an incident energy of 350 MeV measured with an Enge split-pole magnetic spectrograph filled with nitrogen at different pressures as specified (see text for details).

Fig. 3 clearly demonstrates the narrowing of the position spectrum with increasing pressure, which can be described as a charge focusing around a mean charge state characteristic of the ion. The relative narrowing of the spectra can be quantitatively expressed by the ratio $\Delta(B\rho)/\langle B\rho\rangle$ of the full width at half maximum to the average magnetic rigidity. The empirical dependence of the ratio $\Delta(B\rho)/\langle B\rho\rangle$ as a function of pressure is shown in figs. 4a–c for the cases of ^{41}K, ^{58}Ni and ^{126}Te, three ions of interest for AMS experiments. In all three cases, an optimum pressure is obtained where the width of the position spectrum is minimum. The behavior is qualitatively understood as resulting from the competition between the narrowing due to the higher number of collisions with a better statistical averaging of the trajectories and the broadening caused by small-angle scattering and energy loss straggling. Ray-tracing calculations described in detail in section 5 confirm this interpretation. It is interesting to note in fig. 4 that the resolution of the entire charge state spectrum, as measured by the ratio $\Delta(B\rho)/\langle B\rho\rangle$, at the optimum pressure, lies for all measured ions between approximately 1.5–2.5%; this surprisingly good resolution, in view of the broadening action mentioned above, partly results from the large deflection angle (about 115°) of the ions in the Enge split-pole spectrograph.

4. Isobaric separation in a gas-filled magnet and accelerator mass spectrometry measurements

Isobaric (same mass number) ions with the same kinetic energy follow identical trajectories in a magnetic field region in vacuum, for the same ionic charge states. In a gas-filled magnet, the mean charge state of two isobaric ions is different owing to their different nuclear charges; the ions will therefore follow different average trajectories. The actual physical separation of these ions in the focal plane can be very important when a very low intensity group has to be detected and discriminated from a much more intense isobaric group. When the count rate of this group is overwhelming and for example inhibits operation of the focal-plane detector, the isobaric group can be physically blocked before entering the detector. We present in this section the results of several AMS measurements where the gas-filled split-pole spectrograph was used to separate the groups corresponding to long-lived cosmogenic nuclides at extremely low concentrations from a high-intensity isobaric background (see refs. [7,8,12] for details on the AMS measurements).

In order to demonstrate the isobaric separation, a beam of the stable isotopes ^{58}Ni and ^{58}Fe was prepared by using an ion source loaded with a pellet made of

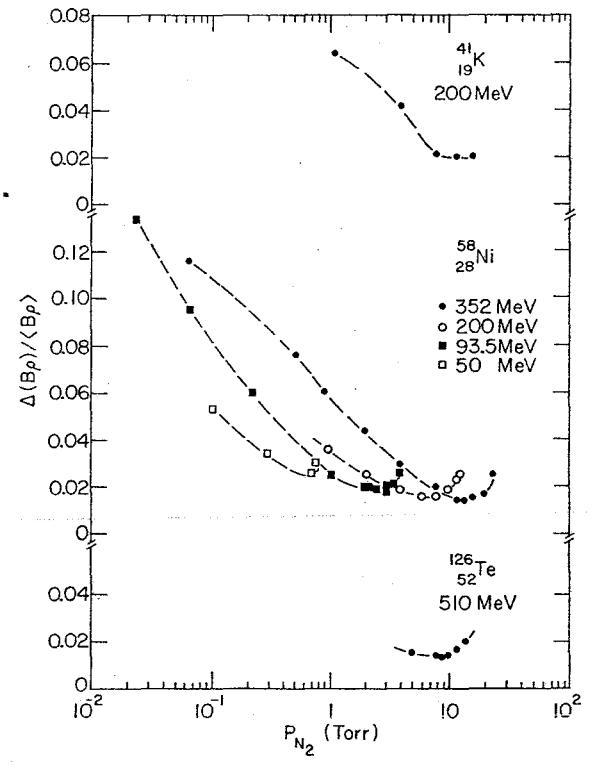

Fig. 4. Empirical dependence of the magnetic rigidity resolution $\Delta(B\rho)/\langle B\rho\rangle$ of the spectrum in the focal plane of the gas-filled split-pole magnetic spectrograph as a function of the gas pressure (nitrogen) for ^{41}K, ^{58}Ni, and ^{126}Te ions at the specified incident energies. The ordinate represented the ratio $\Delta(B\rho)/\langle B\rho\rangle$ of the full width at half-maximum of the focal plane spectra to the average magnetic rigidity. The dashed line connect the experimental points to guide the eye.

mixed Ni and Fe powders and accelerating the ions through the ATLAS system. The $^{58}Ni^{18+}$ and $^{58}Fe^{18+}$ ions behave identically through the accelerating process and emerge with equal kinetic energies (350 MeV). The ions were scattered off a Au foil at 3°, as described in section 3 and analyzed with the split-pole spectrograph, filled with nitrogen at 14 Torr. This pressure is close to the optimal pressure (see fig. 4). The position spectrum (fig. 5) shows a clear separation between the two ions.

Fig. 6 illustrates the application to the isobaric separation between the radioisotope ^{60}Fe and its stable isobar ^{60}Ni. Note that in AMS measurements such as this, the spectrography is positioned at zero degree with respect to the beam and all incident particles are therefore accepted and analyzed. ^{60}Fe is a long-lived isotope ($T_{1/2} = 1.5 \times 10^6$ y) of iron. Its half-life has recently been remeasured by AMS [13] and ^{60}Fe could be an interesting nuclide in meteoritic studies owing to its production in spallation reactions in iron meteorites by galactic cosmic rays. We have made an attempt to detect ^{60}Fe at natural levels using the present method. The major experimental problem is the extremely intense isobaric ^{60}Ni background [14]. The intensity of this group is too high to be allowed to enter the focal plane detector. The separation introduced by the gas-filled spectrograph is large enough that the peak of the ^{60}Ni ions can be physically blocked immediately in front of the focal-plane detector. Fig. 6 shows the spectra obtained by this method; the two-dimensional plot of the ion energy versus position separates the ^{60}Fe group from the tail of ^{60}Ni ions still scattered into the detector, with the main ^{60}Ni peak blocked before entering the detector. The spectra in figs. 6a and 6c were measured for a reference sample with an isotopic abundance of $^{60}Fe/Fe = 5 \times 10^{-9}$. In figs. 6b and 6d we show the spectrum for a sample prepared from the iron meteorite Treysa (fall April 3, 1916) [15]. One single count, identified as ^{60}Fe by its position, energy and specific energy loss, was recorded during a 3 h run, corresponding to a $^{60}Fe/Fe$ ratio of $\sim 3 \times 10^{-14}$. The total number of incident ^{60}Ni isobaric ions separated by the gas-filled magnet in this measurement (shielded from the detector) is estimated to be 4×10^8.

The gas-filled magnet technique was recently applied for the separation of ^{41}Ca from ^{41}K in measurements of ^{41}Ca at natural levels. ^{41}Ca ($T_{1/2} = 1 \times 10^5$ y) has been proposed [16,17] as a possible dating tool for Ca bearing materials (e.g. bones, minerals): ^{41}Ca is expected to be produced in the lithosphere by neutron capture on ^{40}Ca and decay of ^{41}Ca could be a method of measuring ages in the 10^5 y range. The detection of ^{41}Ca at the very low levels expected in nature ($^{41}Ca/^{40}Ca \simeq 1 \times 10^{-14}$) is unfeasible by direct decay measurements and AMS is

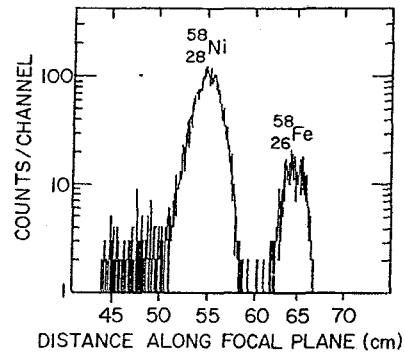

Fig. 5. Separation between two isobaric ions, ^{58}Ni and ^{58}Fe at 350 MeV kinetic energy obtained in the focal plane of the gas-filled split-pole spectrograph. The pressure of the gas (nitrogen) is 14 Torr. The isobaric ions accelerated simultaneously with a charge state of 18^+, were scattered off a Au target at 3° prior to their analysis in the spectrograph (see text).

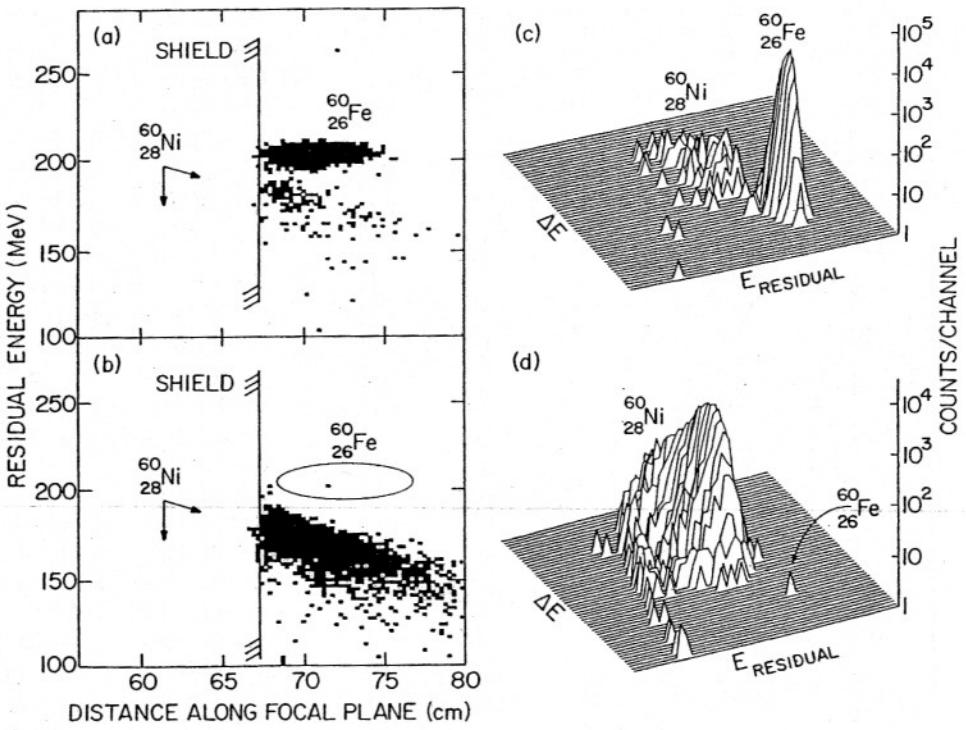

Fig. 6. Isobaric separation between ^{60}Ni and ^{60}Fe ($T_{1/2} = 1.5 \times 10^6$ y) at 340 MeV obtained as in fig. 5 with a gas pressure of 10.5 Torr (nitrogen). The ions in (a) and (c) originate from a reference sample with a concentration ^{60}Fe/Fe $= 5 \times 10^{-9}$, and those in (b) and (d) from a sample prepared from an iron meteorite (Treysa). The main peak of ^{60}Ni, albeit a low-level chemical impurity in the sample, was too intense to be accepted into the focal-plane detector and was blocked by a Ta shield in front of the detector (see fig. 2). In (a) and (b) the residual energy of the ion after passage through the gas is plotted versus its position along the focal plane. The tail of ^{60}Ni particles scattered from the main peak is separated from ^{60}Fe by the measurement of the residual energy. Additional identification of the ions is provided by the specific energy loss, plotted vs the residual energy in spectra (c) and (d). One ^{60}Fe count recorded in the ^{60}Fe region for the natural sample during a 3 h run, corresponds to a ^{60}Fe/Fe isotopic abundance of $\sim 3 \times 10^{-14}$.

at present the only method available. The gas-filled magnet method was used in the first measurement of ^{41}Ca in terrestrial samples of limestone mineral and contemporary bone [18]. Fig. 7 illustrates the performance of the method to separate ^{41}Ca from the interfering ^{41}K stable isobar. The collapse of the charge state spectrum of ^{41}K for different nitrogen pressure, is shown in figs. 7a–c. Figs. 7d–f show the separation obtained for a calibration sample with a known ^{41}Ca concentration and for a calcium sample prepared from a contemporary bovine (long leg) bone from a cow. This material had been pre-enriched in mass $A = 41$ using an electromagnetic separator, thus increasing the ^{41}Ca concentration by a factor of approximately 150. From this value and the ^{41}Ca/Ca ratio measured in the AMS experiment, the original ^{41}Ca isotopic abundance in bone was found to be $(2.0 \pm 0.5) \times 10^{-14}$. In figs. 8a and 8b, spectra from a very recent experiment [19] are shown for a reference sample with a known ^{41}Ca/Ca ratio of 1.44×10^{-12} and for a sample prepared from a limestone mineral respectively. The measurement yields a value of $\sim 3 \times 10^{-14}$ for the ^{41}Ca/Ca concentration in the mineral, a value relatively high compared to the one expected from cosmic ray and natural radioactivity production (see ref. [19] for details and a discussion of the results). It is important to note here that the isobaric separation power of the gas-filled magnet is much higher in a case where the rare nuclide is on the low Z side of the abundant isobar (e.g. $^{60}_{26}$Fe versus $^{60}_{28}$Ni) than in the opposite case. When the rare nuclide has a higher atomic number (e.g. $^{41}_{20}$Ca versus $^{41}_{19}$K), low-energy tails caused by nuclear scattering in the gas or entrance slits and by incomplete charge collection [20] in the ionization detector can produce a non-negligible background. Such events are seen in the bottom part of fig. 8.

Fig. 9 presents the position spectrum obtained for ions from a sample with a ^{126}Sn/Sn concentration of $\sim 1 \times 10^{-7}$. The ^{126}Sn material was separated from fission products in a spent nuclear reactor fuel rod. The possibility to measure the concentration of ^{126}Sn and the specific activity enables one to determine the half-life of the radioactive nucleus. Such a measurement is in

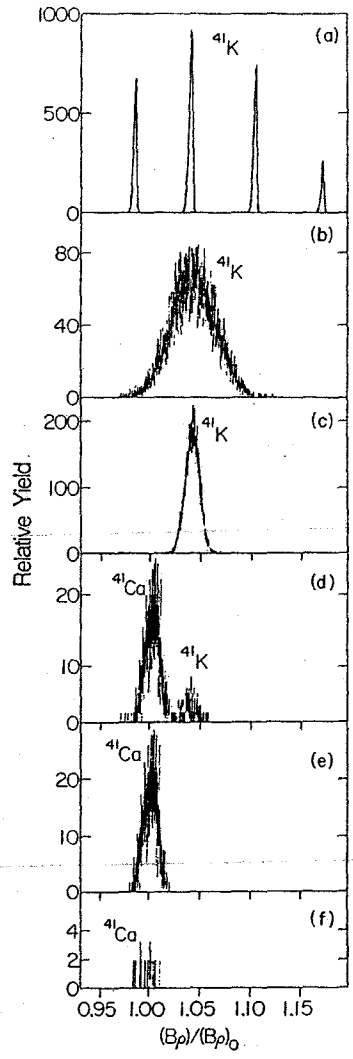

Fig. 7. Position spectra (converted to relative magnetic rigidity $B\rho$), from the focal plane detector of the spectrograph for ^{41}Ca and ^{41}K yields in different samples. The magnetically dispersed charge state spectrum of ^{41}K ions (a) obtained from the passage through a thin gold foil collapsed to a single line when nitrogen gas at pressures of 1.0 Torr (b) or 8.0 Torr (c) was introduced into the magnetic spectrograph. The yields for the gas-filled device at 8.0 Torr from a calibration sample with known concentration (^{41}Ca/Ca = 4.4×10^{-12}) are shown in (d) and (e), and for a pre-enriched (see text) sample prepared from a contemporary bovine (long leg) bone in (f). In (e) and (f) additional gating from the detector total-energy and energy loss signals was applied.

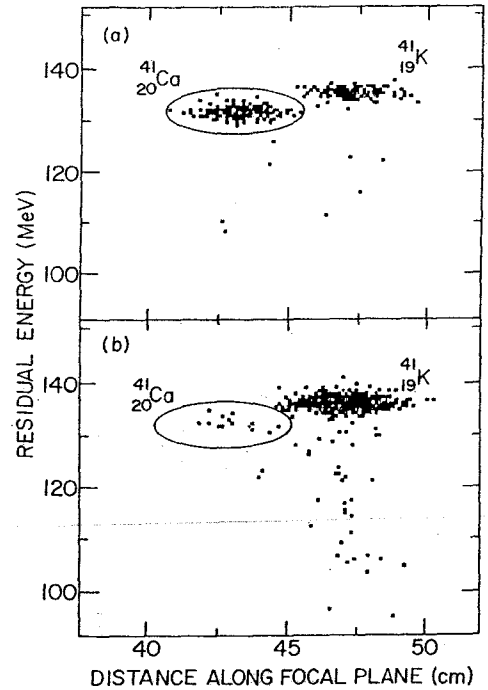

Fig. 8. Two dimensional plot of position vs residual energy for ^{41}Ca and ^{41}K ions accelerated at the ATLAS accelerator with a charge state of 8^+. The isobaric ions are accelerated in an identical way to an energy of 200 MeV and separated in the gas-filled magnetic spectrograph: (a) reference sample with a concentration ^{41}Ca/Ca = 1.44×10^{-12}; (b) a sample of calcium extracted from a limestone mineral with ^{41}Ca/Ca ~ 3×10^{-14}.

5. Semimicroscopic description and Monte Carlo calculations

In this section, we describe a semimicroscopic model for the calculation of the trajectory of an ion in a

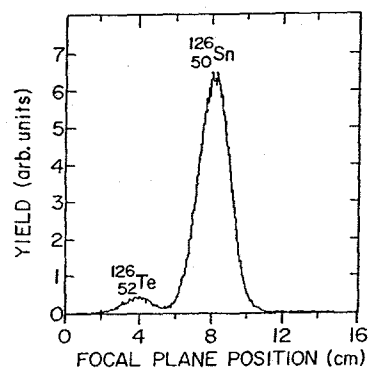

Fig. 9. Separation between 400 MeV isobaric ^{126}Te and ^{126}Sn ($T_{1/2}$ = ≈10^5 y) ions by the gas-filled magnetic spectrograph at a nitrogen pressure of 6 Torr. Measurement of the ^{126}Sn concentration in conjunction with a measurement of the specific activity of ^{126}Sn will yield a new measurement of the ^{126}Sn half-life.

progress at Argonne to determine a more accurate value of the half-life ($T_{1/2}$ ~ 1×10^5 ys). The spectrum (fig. 9) shows that ^{126}Sn can be separated from its stable isobar, ^{126}Te at an energy of 400 MeV.

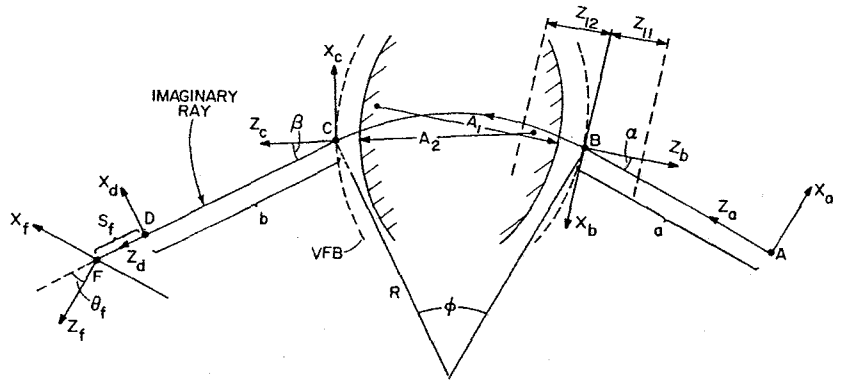

Fig. 10. Schematic representation of a magnetic dipole and definition of the parameters used in the ray-tracing calculations. The points A and D represent respectively the object and image points of the magnet. The distances a and b, outside the fringing field regions (defined geometrically by the virtual field boundary VFB with the distances z_{11}, z_{12}, $\cdots$) are drift spaces. Five different coordinate systems (with origins at A, B, C, D, F) are used in the calculation for the different field regions. In the split-pole magnetic spectrograph, the particles are transported successively through two such dipole pieces. The point F in the figure (corresponding to the second magnetic dipole) represents the intersection between the imaginary ray drawn and the focal surface. The focal-plane detector is placed along the axis x_f.

gas-filled magnet. The model takes into account the charge-changing collision processes. Kinetic energy loss and straggling and the effect of the multiple small-angle scattering, both due to the passage of the ion through the gas, are treated phenomenologically.

5.1. Monte Carlo calculations of the trajectory

The trajectory of the ion is governed by the Lorentz force exerted on the ion in the magnetic field region and by the charge-changing and other collision processes in the gas. The trajectory is calculated here by integrating the equation of motion of the ion with the computer program RAYTRACE [9], using a detailed configuration of the magnetic field regions of the Enge split-pole spectrograph. The definitions of the parameters of the magnetic pole pieces are illustrated in fig. 10 and the values used for these parameters [21] in the present calculations are listed in table 1. The program was modified, as explained below, to incorporate the ion–gas interaction. Denoting by λ the mean free path of the ion between charge-changing collisions, the simulation of the interaction process is performed in a standard Monte Carlo method. At the vertex corresponding to a charge-changing collision, the path length l to the next charge-changing collision is sampled using the relation:

$$l = -\lambda \ln p, \qquad (1)$$

where p is a random number between 0 and 1 and physically represents the probability of the ion surviving a flight path l with no charge-changing collision. At each vertex, the charge state of the ion is modified (see section 5.2) and integration of the equation of motion is continued.

5.2. Charge-changing cross sections

The mean free path λ is related to the total charge-changing cross section σ_t (single- and multiple-electron loss and capture) by the relation:

$$\lambda = 1/n\sigma_t, \qquad (2)$$

where n is the atom or molecule density (in cm^{-3}) of the gas. Cross sections for electron loss and capture depend strongly on the charge state of the ion, its velocity and on the gas. A full knowledge of these quantities would allow one to calculate the probability

Table 1
Parameters of the split-pole magnetic spectrograph used in the Monte Carlo simulation calculations (see fig. 10 for illustration of the geometrical parameters)

	First pole piece	Second pole piece
Object distance (a)	60 cm	14 cm
Image distance (b)	14 cm	60 cm
Pole gap	3.81 cm	3.81 cm
Radius	50.8 cm	50.8 cm
Homogeneous magnetic induction	1.312 T	1.312 T
Magnetic induction in split region	0.176 T	
Deflection angle (ϕ)	40°	74°
Entrance angle (α)	37°	35°
Exit angle (β)	14°	−19°
Entrance curvature (A_1)	−20 cm	infinite
Exit curvature (A_2)	54.1 cm	infinite
Focal plane shift (s_f)		2 cm
Focal plane tilt angle (θ_f)		−41.3°

of any charge-changing process. However, in order to make calculations practical and in view of the often scarce experimental knowledge of the cross sections, especially for fast heavy ions, a model is needed to approximate these quantities.

The cross sections for charge-changing atomic collisions determine the charge-state distribution of the ions in matter. If we denote by F_q the equilibrium charge-state distribution, the following relation exists between F_q and the cross sections $\sigma(q, q')$ for a collision in which the charge state of the ion changes from q to q':

$$0 = \sum_{q \neq q'} \left[\sigma(q, q') F_q - \sigma(q', q) F_{q'} \right], \tag{3}$$

which expresses the fact that F_q is stationary during the transport of the ion in the gas. Equilibrium charge-state distributions of ions in matter have been the subject of many studies, both experimental and theoretical, and several empirical or semiempirical expressions have been developed (see ref. [22] for a recent compilation). Eq. (3) allows one to exploit such expressions in order to derive information on $\sigma(q, q')$. A particularly simple mathematical formulation [22] is obtained if one assumes for F_q a Gaussian shape:

$$F_q = \left(1/d\sqrt{2\pi}\right) \exp\left[-(q - \bar{q})^2 / 2d^2 \right], \tag{4}$$

where $\bar{q}$ denotes the average charge state and d is the standard deviation of the distribution. If one further assumes that only single electrons are captured or lost in the collision processes ($q' = q \mp 1$) and that the dependence of the capture and loss cross sections on the charge state q can be approximated by exponential functions,

$$\sigma_c(q) = A_c \exp[b_c(q - \bar{q})],$$
$$\sigma_l(q) = A_l \exp[-b_l(q - \bar{q})], \tag{5}$$

the following relations are derived from eqs. (3) and (4):

$$1/d^2 = b_c + b_l,$$
$$A_l = A_c \exp[(b_c - b_l)/2]. \tag{6}$$

Multiple electron capture processes have much lower cross sections than single-electron capture, owing mainly to phase space considerations which are confirmed by experimental results [23]. In the present work they were neglected. The parameters A_c and b_c can therefore be obtained by fitting expression (5) for σ_c to electron capture cross sections. Multiple-electron loss processes, on the other hand, have significant cross sections; their effect is to modify the equilibrium charge-state distribution and shift the average charge state to a higher value than would be obtained from single-electron loss processes alone. In order to effectively take into account these processes and yet retain the mathematical simplicity of the previous expressions, the following procedure was used. With the values for $\bar{q}$ and d taken from a semiempirical expression of the equilibrium charge-state distribution F_q (eq. (4)) and the fitted values for the parameters b_c and A_c, effective values for b_l and A_l were derived from eq. (6). This procedure has the advantage of making a direct use of the systematic experimental knowledge on equilibrium charge-state distributions. The expression developed by Dmitriev and Nikolaev [24] for the equilibrium charge state distribution of fast heavy ions in gases was found to best reproduce the experimental results and was used in the calculations. The capture and loss cross sections and the mean free path of the ion are then calculated from the expressions (5) and (2) respectively, defining the total cross section σ_t by:

$$\sigma_t(q) = \sigma_c(q) + \sigma_l(q). \tag{7}$$

At each vertex, the probability for an electron capture (loss) is given by σ_c/σ_t (σ_l/σ_t). The charge-changing cross sections are known to be steep functions of the kinetic energy of the ion in the high-velocity regime $v \gg v_0$, where v_0 denotes the Bohr velocity. The present calculations were made by using the empirical scaling rule developed by Schlachter et al. [25] for the single-electron capture cross sections of fast highly-charged ions in gas targets:

$$\tilde{\sigma}_c = \left(1.1 \times 10^{-8} / \tilde{E}^{4.8}\right)\left[1 - \exp(-0.037\tilde{E}^{2.2})\right] \times \left[1 - \exp(-2.44 \times 10^{-5} \tilde{E}^{2.6})\right]. \tag{8}$$

There $\tilde{\sigma}_c$ and $\tilde{E}$ respectively stand for the reduced capture cross section and the reduced kinetic energy and are defined by:

$$\tilde{\sigma}_c = \sigma_c Z_G^{1.8} / q^{0.5},$$
$$\tilde{E} = E / \left(Z_G^{1.25} q^{0.7}\right), \tag{9}$$

with σ expressed in cm^2 and E in keV/amu. Z_G is the atomic number of the gas. At high reduced energies, σ_c (eqs. (8) and (9)) asymptotically approaches:

$$\sigma_c = 1.1 \times 10^{-8} q^{3.9} Z_G^{4.2} / E^{4.8}. \tag{10}$$

In the course of the calculation, the capture cross sections, calculated from eqs. (8) and (9), are fitted to the expression (5) in order to derive energy-dependent parameters A_c and b_c and those in turn are used, as explained above, to derive the parameters A_l and b_l. For diatomic molecular gases (N_2), the cross sections are first calculated using the atomic number Z_G of the gas and then multiplied by a factor of 2.

5.3. Equation of motion

Between charge-changing collisions in the gas-filled magnet, the ion is submitted to the Lorentz force and to the stopping power dE/dx of the gas. The electronic stopping power, dominant at high velocities, is due to atomic elastic and inelastic collisions which do not

necessarily involve electron capture or loss; the mean free path between such collisions is much shorter than for the charge-changing collisions explicitly treated in the present microscopic model. The (nonrelativistic) equation of motion between two vertices can therefore be written as follows:

$$\mathrm{d}(m\boldsymbol{v})/\mathrm{d}t = q(\boldsymbol{B}\times\boldsymbol{v}) - (\mathrm{d}E/\mathrm{d}x)(\boldsymbol{v}/v). \qquad (11)$$

The stopping power $\mathrm{d}E/\mathrm{d}x$ appearing in eq. (11) differs from the usual stopping power by the fact that the charge state of the ion is not fluctuating between two vertices. $\mathrm{d}E/\mathrm{d}x$ may thus be derived from the charge-state-averaged stopping power $(\mathrm{d}E/\mathrm{d}x)_{\mathrm{ave}}$ by the following relation:

$$\mathrm{d}E/\mathrm{d}x = (q/\bar{q})^2(\mathrm{d}E/\mathrm{d}x)_{\mathrm{ave}}, \qquad (12)$$

where $(\mathrm{d}E/\mathrm{d}x)_{\mathrm{ave}}$ can be taken from stopping power tables [26]. The energy loss straggling due to the fluctuation of the ionic charge state during its flight is thus calculated microscopically by eqs. (11) and (12) when q is allowed to change at each vertex.

5.4. Angle straggling

The angle straggling is introduced by allowing the direction of the velocity vector to be shifted in space at each vertex by an angle δ_Ω. δ_Ω is sampled with a Gaussian distribution:

$$P(\delta\Omega) = N_0 \exp\left(-\delta_\Omega^2/2d_\Omega^2\right), \qquad (13)$$

where d_Ω is the standard deviation. The full width at half-maximum $d_{\Omega 1/2}$ ($d_{\Omega 1/2} = 2d_\Omega\sqrt{2\ln 2}$) was calculated here using a formula [27] based on the Meyer and Sigmund–Winterbon theories of multiple scattering [28–30]:

$$d_{\Omega 1/2} = 1.10\tau^N Z_{\mathrm{ion}} Z_{\mathrm{G}} \tilde{Z}/E, \qquad (14)$$

where $\tilde{Z} = (Z_{\mathrm{ion}}^{2/3} + Z_{\mathrm{G}}^{2/3})^{1/2}$, $\tau = 41.5t/(\tilde{Z}^2 M_{\mathrm{G}})$, $N = [\ln(1.03+\tau)]^{-0.115} - 0.115$, t (in $\mu\mathrm{g/cm^2}$) being the thickness of the gas between two collisions and M_{G} (in amu) the atomic mass of the gas. E (in MeV) is the kinetic energy of the ion. In the calculations, t was taken as the thickness corresponding to one mean free path.

5.5. Calculations and comparison to experimental data

The simulation calculations were made by transporting a large number of incoming ions with randomly sampled (x_a, y_a) and (θ_a, ϕ_a) coordinates (θ_a and ϕ_a are the polar and azimuthal angles of the velocity vector) around the object point A of the first dipole ($z_a = 0$; see fig. 10) onto the focal plane of the split-pole magnetic spectrograph. The initial charge state of the ion is sampled with an equilibrium charge state distribution in solids in order to simulate the effect of the entrance window in the gas-filled region. The expression developed by Sayer [31] for the charge state distribution for fast heavy ions in solids was used and found to reproduce adequately the experimental results. Position and energy spectra were generated with the previously described transport model by accumulating the coordinates (x_f and y_f) in the focal plane and the residual energy of the ion. An example of calculated position spectra in the focal plane and their evolution with gas pressure are shown in fig. 11 and can be compared with the experimental spectra of fig. 3. Fig. 12 shows a comparison between the calculated and experimental resolution $\Delta(B\rho)/\langle B\rho\rangle$ as a function of gas pressure

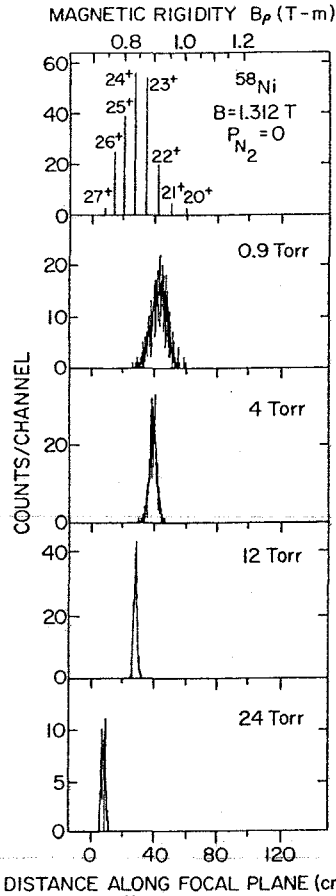

Fig. 11. Position spectra calculated by Monte Carlo simulation, as explained in text, for ^{58}Ni ions in the gas-filled split-pole magnetic spectrograph. Note the shift in the position of the centroid between the spectrum in vacuum ($P = 0$) and at 0.9 Torr, corresponding respectively to the mean charge state of the ions after passing through the Mylar entrance foil of the magnet and the mean charge state in the gas. At higher gas pressures, the centroid of the group is moving towards smaller magnetic rigidities because of the energy loss in the gas. A similar behavior is observed in the experimental spectra in fig. 3.

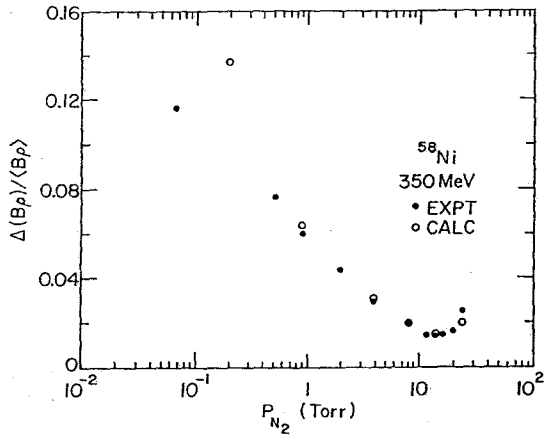

Fig. 12. Comparison between the calculated and experimental resolution in magnetic rigidity $\Delta(B\rho)/\langle B\rho\rangle$ for ^{58}Ni ions. See caption in fig. 4 for the definition of $\Delta(B\rho)/\langle\beta\rho\rangle$. The calculation is seen to agree well with the experimental points above 1 Torr.

for ^{58}Ni ions; the calculation reproduces satisfactorily the position of a minimum caused by the competing contributions from the charge state averaging and from broadening due to small-angle scattering. Some ion trajectories in the magnet, calculated for the case of ^{58}Ni, are shown in fig. 13.

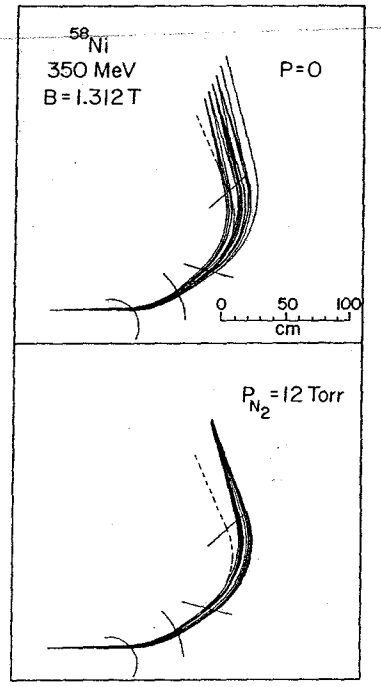

Fig. 13. Calculated trajectories for ions in the split-pole spectrograph in vacuum (top) and filled with nitrogen at 12 Torr (bottom). The four lines transverse to the trajectories represent the pole faces of the two dipoles. The dashed lines represents the central geometrical ray of the spectrograph.

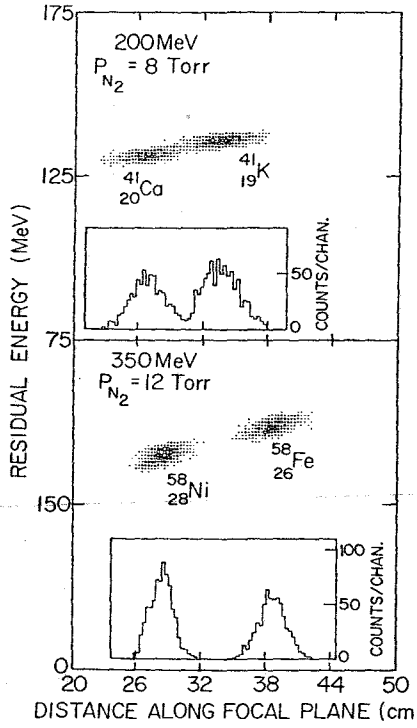

Fig. 14. Calculated two-dimensional spectra of residual energy vs position along the focal plane for isobaric pairs ^{41}K–^{41}Ca (top) and ^{58}Ni–^{58}Fe (bottom) at the specified energies. The inserts show the projection of the groups along the focal plane axis. The plots reproduce the physical separation along the focal plane and the difference in residual energy of the isobaric ions due to the difference of the energy losses in the gas. Within each group, a correlation between residual energy and position can be seen. The plots can be compared to the experimental spectra in figs. 5 and 8.

Calculated two-dimensional plots of the residual energy of the ion after the passage through gas versus position along the focal plane are illustrated in fig. 14 for the cases of the ^{41}K–^{41}Ca and ^{58}Ni–^{58}Fe isobaric pairs. The spectra are in good agreement with those observed in the experiments (see figs. 5–8); the isobaric groups are separated in position and in residual energy because of the different energy losses of the ions in the gas.

6. Behavior of the gas-filled split-pole spectrograph at low pressures

The position spectra measured along the focal plane at intermediate pressures (in the 10^{-3}–10^{-2} Torr range) show interesting features. As can be seen in figs. 3b and 3c for ^{58}Ni ions, at these pressures the discrete charge states of the ion maintain their identity and appear as peaks with positions unshifted relative to the spectrum

in high vacuum (fig. 3a); these peaks correspond to ions which have not suffered any charge-changing collisions throughout their path. However, events are observed between the peaks, corresponding to particles which have undergone interaction in the gas. Such particles are likely to have had one and only one collision during their path since the mean free path in this pressure range is not small compared to the length of the trajectory ($\lambda \simeq 135$ cm for a gas pressure of 0.02 Torr).

Especially striking in these spectra is the appearance of small side peaks, principally to the left of the main charge state peaks. These peaks are interpreted as corresponding to ions having undergone a charge-changing collision within the split region between the two pole pieces of the spectrograph (see fig. 2). In this region, the magnetic field is low (approximately 13% of the value of the homogeneous field in the gaps) and the corresponding deflection of the ions through the low-field region is negligible (see the ion trajectories in fig. 13). Therefore all ions which undergo a collision in this region will accumulate at the same position in the focal plane. Moreover, since the main deflection angle of the ions occurs in the second pole piece (fig. 13), one can attribute a peak situated close to and at the left side of the main charge state q, to particles with initial charge state $q+1$ and having undergone a $q+1 \rightarrow q$ (electron capture) collision within the low-field region. The overall deflection is therefore close to but larger than that of a particle with initial charge state q. The experimental spectrum confirms that multi-electron capture collisions are much less frequent. It is also clear from the spectrum that groups corresponding to electron loss collisions are much weaker and barely visible. This stems from the fact that the initial charge state distribution of the ions upon entering the magnet is determined by the solid (Mylar) entrance foil. The charge-changing reactions occurring in the gas, however, tend to bring the ion charge states towards a new distribution characteristic of the interaction with the gas. This distribution is known to be centered around a mean value smaller than that in the solid and consequently electron capture reactions are very much favored.

It is interesting to note that the appearance of the electron capture peaks can be reproduced by a detailed Monte Carlo simulation, as described in section 5.1. Fig. 15 illustrates such a calculation for 350 MeV ^{58}Ni ions at a gas pressure of 0.02 Torr and its comparison with the experimental spectrum of fig. 3c). Both the experimental and calculated spectra show peaks corresponding to electron capture reactions of ions at charge states 26+, 25+, 24+, 23+ and 22+ to 25+, 24+, 23+, 22+ and 21+ charge states respectively. Peaks corresponding to electron loss reactions are not seen in the calculated spectrum.

The behavior of the split-pole spectrograph at low gas pressures seems therefore to provide a powerful tool

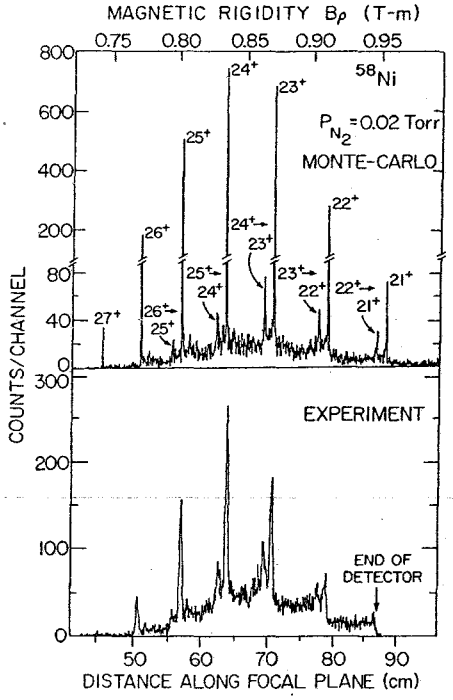

Fig. 15. Experimental (bottom) and calculated (top) spectra of the position along the focal plane for 350 MeV ^{58}Ni ions transported through the split-pole spectrograph filled with nitrogen gas at a pressure of 0.02 Torr. The side peaks adjacent to the main charge states originate from electron capture atomic collisions (as specified in the top part) between the ion and the nitrogen gas molecules within the low-field split region of the spectrograph.

to study electron capture (and maybe also electron loss) atomic collisions. Owing to the broad-range capability of the instrument, it may become feasible to measure with a single magnetic field setting, the cross sections of the different charge-changing reactions.

7. Conclusion

The properties of an Enge split-pole magnetic spectrograph filled with gas have been studied for the case of several fast heavy ions. Special emphasis was given to the separation power of the instrument for pairs of isobaric ions; it was shown that the spatial separation provided by the gas-filled magnet for such ions which have ion-optically degenerate trajectories in vacuum can be a decisive factor. This is the case for example in accelerator mass spectrometry experiments which aim to measure extremely small isotopic abundances, often in the range of 10^{-12} to 10^{-15}. It was shown that the gas-filled magnet provides a means to reject very high intensities of isobaric background. This property will probably become even more valuable with the develop-

ment and use of new-generation high-intensity sources of negative [32] and positive [33] ions, which are expected to increase the sensitivity in AMS measurements. A particularly interesting aspect of the gas-filled method yet to explore is its extension to isobar separation at much lower energies which would make it a valuable tool for accelerator mass spectrometry with small accelerators [34]. The particular behavior of the gas-filled split-pole magnet at low gas pressures in the regime where single atomic collisions occur within the ion flight path, is pointed out. The specific configuration of the instrument allows the identification of single charge-changing atomic collisions (mainly single- and multiple-electron capture) between the ion and gas molecules, which could be utilized for the measurement of their cross sections.

Acknowledgements

We should like to thank E. Kanter for helpful discussions an atomic physics problems. This work was supported in part by the USA–Israel Binational Science Foundation.

References

[1] C.B. Fulmer and B.L. Cohen, Phys. Rev. 109 (1958) 94.
[2] P. Armbruster, Nukleonik 3 (1961) 188.
[3] K. Sistemich, J.W. Grueter, H. Lawin, J. Eidens, R. Fabbri, T.A. Khan, W.D. Lauppe, G. Sadler, H.A. Selic, M. Shaanan and P. Armbruster, Nucl. Instr. and Meth. 130 (1975) 491.
[4] W. Henning, M. Paul, W. Kutschera, K.E. Rehm and R.H. Siemssen, Bull. Am. Phys. Soc. 30 (1985) 1249.
[5] H. Miyatake, T. Nomura, H. Kawakami, J. Tanaka, M. Oyaizu, K. Morita, T. Shinozuka, H. Kudo, K. Sueki and Y. Iwata, Nucl. Instr. and Meth. B26 (1987) 309.
[6] A. Ghiorso, S. Yashita, M.E. Leino, L. Frank, J. Kalnins, P. Armbruster, J.-P. Dufour and P.K. Lemmertz, Nucl. Instr. and Meth. A269 (1988) 192.
[7] A.E. Litherland, Ann. Rev. Nucl. Part. Sci. 30 (1980) 437.
[8] D. Elmore and F.M. Phillips, Science 236 (1987) 543.
[9] J.E. Spencer and H.A. Enge, Nucl. Instr. and Meth. 49 (1967) 181.
[10] H.A. Enge, Nucl. Instr. and Meth. 162 (1979) 161.
[11] J.R. Erskine, T.H. Braid and J.C. Stolzfus, Nucl. Instr. and Meth. 135 (1976) 67.
[12] W. Henning, W. Kutschera, M. Paul, R.K. Smither, E.J. Stephenson and J.L. Yntema, Nucl. Instr. and Meth. 184 (1981) 247.
[13] W. Kutschera, P.J. Billquist, D. Frekers, W. Henning, K.J. Jensen, X. Ma, R. Pardo, M. Paul, K.E. Rehm, R.K. Smither and J.L. Yntema, Nucl. Instr. and Meth. B5 (1984) 430.
[14] W. Kutschera, Nucl. Instr. and Meth. B17 (1986) 377.
[15] We gratefully acknowledge the assistance of P. Englert in making an iron sample from the Treysa meteorite available to us.
[16] Y. Yamaguchi, Prog. Theoret. Phys. 30 (1963) 567.
[17] G. Raisbeck and F. Yiou, Nature (London) 277 (1979) 42.
[18] W. Henning, W.A. Bell, P.J. Billquist, B.G. Glagola, W. Kutschera, Z. Liu, H.F. Lucas, M. Paul, K.E. Rehm and J.L. Yntema, Science 236 (1987) 725.
[19] W. Kutschera, I. Ahmad, P.J. Billquist, B.G. Glagola, K. Furer, R.C. Pardo, M. Paul, K.E. Rehm, P.J. Slota, R.E. Taylor and J.L. Yntema, Proc. 13th Int. Radiocarbon Conf., Dubrovnik, Yugoslavia (1988) to be published in Radiocarbon.
[20] T.R. Ophel, L.K. Fifield, W.N. Catford, N.A. Orr, C.L. Woods, A. Harding and G.P. Clarkson, Nucl. Instr. and Meth. A272 (1988) 734.
[21] H.A. Enge, private communication.
[22] H.D. Betz, Appl. At. Collis. Phys. 4 (1983) 1.
[23] J.R. Macdonald, S.M. Ferguson, T. Chiao, L.D. Ellsworth and S.A. Savoy, Phys. Rev. A5 (1972) 1188.
[24] I.S. Dmitriev and V.S. Nikolaev, Zh. Eksp. Teor. Fiz. 47 (1964) 615. [Sov. Phys.-JETP 20 (1965) 409].
[25] A.S. Schlachter, J.W. Stearns, W.G. Graham, K.H. Berkner, R.V. Pyle and J.A. Tanis, Phys. Rev. A27 (1983) 3372.
[26] F. Ziegler, The Stopping Power and Ranges of Ions in Matter (Pergamon, New York, 1978).
[27] K. Green and D. Burch, U. of Washington Annual Report (1975) unpublished.
[28] L. Meyer, Phys. Stat. Sol. (b) 44 (1971) 253.
[29] L. Meyer, M. Klein and R. Wedell, Phys. Stat. Sol. 83 (1977) 451.
[30] P. Sigmund and K.B. Winterbon, Nucl. Instr. and Meth. 119 (1974) 541.
[31] R.O. Sayer, Rev. Phys. Appl. 12 (1977) 1543.
[32] R. Middleton, Nucl. Instr. and Meth. 214 (1983) 139.
[33] R. Geller, B. Jacquot and M. Pontonnier, Rev. Sci. Instr. 56 (1985) 1505.
[34] P.W. Kubik, D. Elmore, T.K. Hemmick and W. Kutschera, Proc. Conf. on Application of Accelerators in Research and Industry, Denton, Texas (1988) to be published in Nucl. Instr. and Meth. B.